HMI ring diagram analysis I. The processing pipeline

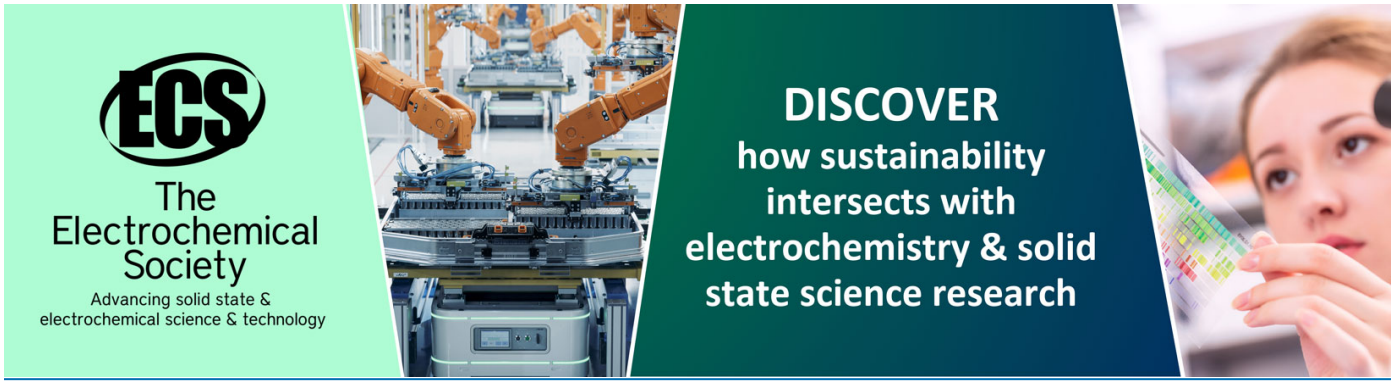

Journal of Physics: Conference Series **271** (2011) 012008 doi:10.1088/1742-6596/271/1/012008

HMI ring diagram analysis I. The processing pipeline

R. S. Bogart[1], C. Baldner[2], S. Basu[2], D. A. Haber[3] and M. C. Rabello-Soares[1]

[1] Stanford University, Stanford, Calif. USA
[2] Yale University, New Haven, Conn. USA
[3] JILA, University of Colorado, Boulder, Colo. USA

E-mail: rbogart@stanford.edu

Abstract. The combination of high resolution, spatial coverage, and continuity of photospheric Doppler and other data from HMI has allowed us to embark on a program of systematic exploration of solar subsurface flows and thermal structure variations using the technique of ring-diagram analysis on an unprecedented scale. Two ring-diagrams pipelines exist: a synoptic program aimed at mapping the evolution of the circulation and local subsurface flows on a global scale from the surface to depths of down to $0.9R_sun$, and a targeted program designed to provide a comprehensive view of the thermal structure anomalies associated with loci of magnetic activity over the course of their life cycles. In this paper we describe the analysis techniques implemented in the processing pipelines.

1. Introduction

Two ring-diagram pipelines are being developed: one producing synoptic views of the flows and structure on regular spatial grids, and the other producing detailed flow and structure anomalies associated with specific target regions. We will refer to these as the "synoptic" and "target" pipelines, respectively. Both have common requirements for most of the analysis modules and data structures, so it is appropriate to consider them together.

The HMI ring-diagram analysis pipelines consist of several distinct elements. Each of these pipeline elements is described in a section below. Fuller documentation on the pipeline analysis modules and associated data products can be found on the web pages of the HMI Ring Diagrams Team, at *http://hmi.stanford.edu/teams/rings/*.

The primary analysis dataset for the standard pipelines is the set of full-resolution full-disc Dopplergrams produced by the HMI Observables Pipeline at a cadence of one per 45 sec. However, ring-diagram pipelines have been run on other observables as well, including continuum intensity and line depth.

2. Quality checks and coverage

HMI data coverage has been almost continuous since 1 May 2010 and is expected to remain so. Occasional images are unsuitable for inclusion in the processing pipeline for various reasons, usually because the Image Stabilization System was turned off for instrument calibrations, occasionally for other reasons such as transmission or processing errors. These do not generally amount to more than a fraction of a percent of the total, so low duty cycle is not an issue. The pipelines have, however, been used to process earlier test data sequences as part of the instrument

calibration, so it was necessary to include data coverage checks. The module **rdcover** reports the available duty cycle for the input data using the same target interval and rejection criteria as the tracking. With MDI data it was established that data coverages of less than 0.85 led to degradation in the quality and number of fits, and those less than 0.70 led to serious degradation. These numbers may be conservative for HMI, but will be irrelevant except in the case of spacecraft emergencies or for shorter analysis intervals around the times of eclipses.

Sufficient data are available to the HMI observables processing for reliable and useful quality flags to be set on the individual output records. The tracking module can reject images from a hand-prepared list as well as on the basis of their quality flags. We have been visually inspecting the observable image statistics and updating a rejection list to trap cases in which automatic quality assessment failed. As those cases are understood and the observables code matures, this step should become unnecessary. The tracked data cubes include in their associated metadata log files identifying the input images which were rejected and interpolated over.

3. Data averaging

Spatial variations in the Doppler signal are removed before analysis by subtracting a long-term mean. These variations are primarily due to the solar rotation of course, but there are also effects due to the non-uniform response of the instrument; an example of the latter are the "fringes" which are actually in the lookup tables for the Doppler calibration based on integrated-light observing sequences in which the front window rather than the Sun is imaged. As regions are tracked across the field of view such spatial variations acquire a temporal component.

The Doppler data have a very large diurnal variation due to the orbital motion of the spacecraft. The orbital velocity must be removed from both the temporal averages and the individual images as they are tracked. The module **datavg** is used to produce such corrected averages over one-third of a Carrington rotation (about 9 days), sampled six times per rotation. Data series produced by this module such as **hmi.V_avg120** are available to the tracking module for background subtraction. The synoptic pipeline requires them, creating the appropriate records if they do not already exist.

4. Target generation

The synoptic data products for transverse velocities are sampled at a spatial scale corresponding to $2^\circ.5$ heliographic (~ 30 Mm), with analysis regions of diameter 5°, extending out to $\mu = 0.986$, about 80° from disc center. At this distance the area of foreshortened HMI pixels is comparable to that of the limit at which we were able to extract useful ring-diagram fits from full-disc MDI data at one-third the spatial resolution.

To invert for velocities and structure below the immediate sub-surface layers, we must sample larger areas for longer intervals as well, as the small regions can only resolve the lowest order modes, the spatial and temporal Nyquist frequency being comparatively high. We also analyse on $7^\circ.5$ and 15° sampling grids, with the regions again having diameters twice the grid spacing. Because we sample so close to the limb, the annual variation of heliographic latitude on the ecliptic provides an opportunity to measure at least the smaller tiles at higher latitudes during part of the year. We divide the year into four grid "seasons" at the times when $B_0 = \pm 3^\circ.625$. (The two extreme cases are mirror images of one another in latitude.) Our ability to reach near the limb and a desire to keep the tiles approximately equally spaced regardless of latitude leads to a rather complicated selection of the target locations in heliographic latitude and Stonyhurst longitude (*i.e.* referred to geocentric central meridian) for the smaller tiles. The program **gentargs** generates the appropriate list of target latitudes and longitudes for a given time to be used as parameters for the tracking module.

The temporal sampling intervals correspond to the time it takes a region to rotate through its diameter, 5° of Carrington rotation (1/72 of a synodic rotation, 545 min) for the 5° tiles,

and correspondingly longer for the larger tiles — 1/24 and 1/12 of a synodic rotation (1635 min and 54.5 hr), respectively. The actual tracking times are somewhat longer: 576, 1728, and 3456 min, respectively, to allow for modest apodization of the power spectra.

For the target pipeline, we compare results for the region of interest compared with those for one or more other regions observed under as close to the same conditions as possible. In practice, that means selecting comparison regions at the same latitude and within about 120° longitude. The comparison regions are selected on the basis of their Magnetic Activity Index (MAI, described in the next section) being as low as possible within the location constraints. Region sizes and tracking times for the target pipeline are still to be determined. We plan to begin with 15° regions tracked for 1/12 or 1/6 of a Carrington rotation, as has been done with MDI.

5. MAI determination

In the past the Magnetic Activity Index has been determined by mapping and tracking regions of the same geometry from MDI magnetograms and integrating the unsigned flux exceeding a certain threshold, based on the noise characteristics of the instrument. While MDI and HMI are co-observing that is still being done, but we will obviously have to convert to a new MAI based on HMI magnetograms. We expect to use the same method, but the selection of parameters for noise thresholds and sampling rates must be adjusted for the different observations. The module **maicalc** is still under development, but this only affects the implementation of the target pipeline.

6. Tracking

Region definition in time and space is at the heart of local-area helioseismology. The ring-diagram pipelines, as well as the time-distance pipeline, use the module **mtrack** to convert a time-sequence of solar images to a collection of three-dimensional data cubes, each representing the data for a particular target region. If the region is centered at fixed heliographic coordinates, this implies tracking at the Carrington rotation rate, and this is what is done for the HMI ring diagram pipelines. (Ring-diagram analysis of MDI and GONG data has been done traditionally with regions at different latitudes tracked at different rates, approximating the differential rotation rates in photospheric Doppler signal at the latitudes involved.) Image data are mapped from their surface spherical coordinates to the plane using Postel's azimuthal equidistant projection, interpolated from the image plane with a cubic convolution kernel. In the synoptic pipeline the map scale at center of each region is 0°.04 per map pixel for the 5° and 15° tiles, corresponding roughly to the image scale at disc center, 0°.08 for the 30° tiles. With spatial extents of 128, 384, and 384 pixels, the tracked cubes have a full extent of 5°.12, 15°.36, and 30°.72 respectively, allowing for circular spatial apodization of the power spectra to the target radii.

Region parameters in the target pipelines have not been defined, and may not be rigid. Initial tests have been with 15° tiles tracked with similar parameters as for the synoptic pipeline, but for twice the duration.

We plan eventually to track each of the target regions for their full disc passages, and then to extract from those long data cubes the intervals needed for each analysis period. This will reduce the number of times that the input data files need to be read. For now, each region is tracked from original data for each analysis period. The tracking module does create multiple cubes for different regions from the same input data set, but system limits constrain the number of regions that can be tracked concurrently to about 250. For the 5° synoptic series, in which over 2700 regions must be tracked every 9 hours, this is a particular issue.

7. Power spectra

Power spectra are calculated via a straightforward 3-d Fourier transform of the real data in the tracked cubes, using the **pspec3** module. The data are apodized with a 4-th order polynomial taper in both the spatial and temporal dimensions. The radial apodization varies from unity at the target radius to zero at the edge of the map. For the map sizes and scales used in the pipeline, that is a fractional distance of 0.0234375 of the map width. The temporal apodization is from 0 at the endpoints to 1 over a distance of 0.015625 of the total interval.

The power spectra are normalized so that the integrated power over all voxels in the power spectrum is equal to the variance of the original data cube. To convert the power spectral density to physical units, one must divide by the physical scales (CDELTi) of the power spectrum.

8. Ring fitting

We have two different algorithms for parametric fitting of the "rings", ridges in the 3-d power spectrum. Module **rdfitc** implements the approach of [1], in which fits to a 13-parameter model including multiple background and asymmetry terms are performed for each point in selected temporal frequency planes of the power spectrum, with generation of a full covariance matrix. This method provides more reliable parameter estimates, but is comparatively time-consuming. Module **rdfitf**, based on the approach of [4], fits only 6 parameters in the frequency dependence of the lowest order azimuthal Fourier terms of the azimuthally analysed spatial power spectrum. It is very fast and well-suited to the determination of the U_x and U_y terms needed for flow inversions; but the frequency determinations are not as reliable.

For the synoptic pipeline, the fast fitting is applied to all regions. For the 15° and 30° tiles comprehensive fits are done only for the tiles on central meridian. We are currently doing comprehensive fits for all of the 5° tiles, since their small size permits this (the fitting time varies roughly as the 4th power of the cube sizes). Once we have gained sufficient confidence in the results we will likely abandon one of these two otherwise redundant sets of fits.

Only the comprehensive fits are performed for the target pipeline, as the inversions depend sensitively on the mode frequency determinations.

9. Inversions

The two parameters U_x and U_y, representing horizontal displacement of the centers of the rings in the frequency plane corresponding to different modes, are inverted for the depth dependence of the transverse velocity of the observed field (relative to the tracking rate!) using the OLA procedure described in [1]. The inversion is implemented in module **rdvinv**.

For the structure pipeline frequency differences between comparison regions are inverted for sound-speed and adiabatic gradient variations with depth, as described in [3]. Inversions for thermal structure perturbations are not yet implemented in the synoptic pipeline, because of the lack of an appropriate set of quiet-Sun reference frequencies over the disc.

Full three-dimensional flow inversions from combinations of the synoptic analysis regions at all scales are planned, but these techniques are still under development.

Acknowledgments

This work was supported in part through NASA grants NAS5-02139, NNX09AB04G, and NNX07AH82G.

References

[1] Basu S and Antia H.M 1999 *Astrophys. J.* **525** 517
[2] Basu S, Antia H.M and Bogart R S 2004 *Astrophys. J.* **610** 1157
[3] Bogart R S, Basu S, Rabello-Soares M C and Antia H.M 2008 *Solar Phys.* **251** 439
[4] Haber D A, Hindman B W, Toomre J, Bogart R S, Thompson M J and Hill F 2000 *Solar Phys.* **192** 335